Evaluation of cross-sectional deformation in pipes using reflection of fundamental guided waves

Citation for published version:
Zhou, C, Xu, ZD, Lu, H & Lu, Y 2022, 'Evaluation of cross-sectional deformation in pipes using reflection of fundamental guided waves', *Journal of Engineering Mechanics*, vol. 148, no. 5, 04022016, pp. 1-16. https://doi.org/10.1061/(ASCE)EM.1943-7889.0002095

Digital Object Identifier (DOI):
10.1061/(ASCE)EM.1943-7889.0002095

Link:
Link to publication record in Edinburgh Research Explorer

Document Version:
Peer reviewed version

Published In:
Journal of Engineering Mechanics

Evaluation of cross-sectional deformation in pipes using reflection of fundamental guided waves

Chen Zhu[1], Zhao-Dong Xu, A. M. ASCE[2*], Hongfang Lu, A. M. ASCE[3], Yong Lu, F. ASCE[4]

Abstract: Ultrasonic guided wave technology has been successfully applied to detect multiple types of defects in pipes. However, cross-sectional deformation, which is a common defect, is less studied as compared to structural discontinuity defects in pipes. In this paper, the guided wave is employed to detect cross-sectional deformation. First, the effect of section deformation parameters on the reflection of guided waves is analyzed using a series of three-dimensional finite element (FE) models, and the deformation parameters affecting the reflection are examined in light of the physics of the guided waves based on the FE results. The results show that the reflection occurs at the start of the cross-sectional deformation, while the subsequent gradual deformation region does not cause reflection. The reflection coefficient is dependent on the axial deformation severity and the mode conversion ratio is dependent on the circumferential deformation extent. Secondly, an experimental study was conducted to evaluate the guided wave reflection characteristics due to the pipe cross-sectional deformation in a realistic situation. Test pipes with local and overall deformation cases were manufactured, and the reflection from both types of deformation was investigated experimentally. The results show good agreement between the experimental measurement and FE prediction. Two quantitative parameters, namely axial deformation rate δ and circumferential deformation rate β are defined to represent the cross-sectional deformation, and these parameters are found to well correlate with the reflection

coefficient and mode conversion ratio. The ratio of δ/β is suitable to be used to judge the deformation type.

Keywords: Ultrasonic guided waves; Cross-sectional deformation; Deformation parameters; Reflection coefficient; Mode conversion ratio.

Authors:

[1] Ph.D. Candidate, China-Pakistan Belt and Road Joint Laboratory on Smart Disaster Prevention of Major Infrastructures, Southeast University, Nanjing 210096, China. E-mail: zhchen_cz@163.com

[2] Professor, China-Pakistan Belt and Road Joint Laboratory on Smart Disaster Prevention of Major Infrastructures, Southeast University, Nanjing 210096, China (corresponding author). E-mail: zhdxu@163.com

[3] Associate Professor, China-Pakistan Belt and Road Joint Laboratory on Smart Disaster Prevention of Major Infrastructures, Southeast University, Nanjing 210096, China. E-mail: luhongfang@seu.edu.cn

[4] Professor, Institute for Infrastructure and Environment, School of Engineering, The University of Edinburgh, Edinburgh EH9 3 JL, UK. E-mail: yong.lu@ed.ac.uk

Introduction

Deformation defect is one of the major defects in pipelines (Shan et al. 2018), and such defect is mainly caused by excessive local stress (Ni and Mangalathu 2018). Typical pipe deformations such as dent and bulge reduce the transport efficiency and weaken the pipe structure's normal load-bearing capacity. Stress concentration and section weakening caused by the abrupt change in its shape can make the deformed part prone to failure and leakage (Lam and Zhou 2016). Current methods for pipe deformation detection are primarily based on visual inspection (Lu et al. 2021). These methods require good visual conditions and access to the inside of the pipe, which is difficult to satisfy in some practical situations (Duran et al. 2003; Kim et al. 2003).

Ultrasonic guided wave technology has been applied to the nondestructive testing of the plate, pipeline, rail, etc (Wang and Yuan 2005; Alleyne et al. 2001; Hayashi et al. 2004). It is owing to its advantages in local excitation and reception, full cross-section detection and long-distance detection capabilities. Compared with the damage identification methods that are based on the vibration modes of the structure (Xu and Wu 2007; Xu et al. 2011; Xu and Wu 2012; Wang et al. 2016), the ultrasonic guided wave technology does not require the installation of transducers for the entire length of the pipe, and damage over a long-distance along the pipeline can be detected by a single transducer on the pipe surface (Xu et al. 2021). In addition, guided wave technology is more sensitive to small defects, which overcomes the difficulties of detecting pipeline damage with traditional dynamics methods (Xu et al. 2015; Xu et al. 2018; Ge et al. 2022).

Ultrasonic guided wave technology uses the interaction of guided waves with the discontinuities in the geometry of the waveguide. The information related to damage characteristics can be extracted from reflected guided waves. The interaction between guided waves and structural discontinuities has attracted wide attention in the research community. Demma et al. (2003;2004) carried out a systematic study on the interaction of guided waves with simulated rectangle corrosion damage in pipelines, and they investigated the effects of pipe size, defect size, guided wave mode, and frequency on reflection from the notches. Carandente et al. (2010) studied the reflection of T(0,1) (first order torsional mode) guided wave with simulated tapered step notch. They analyzed the effects of different contours and depths on the reflection coefficients. A method was proposed to evaluate the damage depth according to the damage circumferential range and the maximum reflection coefficient (Carandente and Cawley 2012). Lovstad and Cawley (2011;2012) analyzed the effect of circular holes on T(0,1) reflection in the pipes to study pitting corrosion and proposed a method to evaluate the corroded area.

Research on the assessment of pipeline deformation based on guided wave technology has been rather limited. In general, the pipe deformation may be divided into a) the overall deformation, such as bend, and b) the local section deformation, such as dent. For pipe bends, Demma (2001) studied the mode conversion of longitudinal and torsional modes due to the existence of bends in the pipe and the effects of bend radius and length. Verma B et al. (2014) used the L(0,2) (second-order longitudinal mode) to study bending pipes with different bending angles and bending radii. The transmittance and mode conversion laws of pipes with different bending angles were summarized, and the influence of bending pipes with different wall thicknesses on mode conversion was also examined. Zhang et al. (2020) studied the detection of sizeable bending angle deformations of the pipeline caused by external force. The in-plane shear piezoelectric can obtain the shear deformation due to bending, and the sensor locations can deduce the bending direction in the pipeline. For local pipe dent, Na and Kundu (2002) used the array ultrasonic transducer to excite the flexural mode guided wave in the underwater pipeline to detect the deformation damage, focusing on the effect of the different incident angles of ultrasonic transducers and frequencies on the received signal amplitude. Ma et al. (2014) studied the reflection of L(0,2) guided wave on dent deformation. They introduced an ellipticity parameter to evaluate the degree of deformation and studied the effect of deformation degree on reflection. However, the relationship between deformation parameters and the reflection characteristics has not been fully investigated. There is also no unified definition of the parameters that characterize the cross-sectional deformation in the pipe.

This paper aims to investigate the guided wave reflection from cross-sectional deformation defect, and attempts to establish the relationship between reflection characteristics and geometric deformation parameters. The mode and frequency range selection are discussed in Section "Mode characteristics and frequency range of guided waves". Section "Finite element modeling" presents a numerical simulation study using finite element models. The analysis starts with the reflection from axisymmetric model in Section "Axisymmetric finite element modelling". The reflection from non-axisymmetric model is shown in Section "Non-axisymmetric finite element modelling". In light of the physics of guided waves and FE results, the deformation parameters affecting the reflection coefficients and mode conversion are discussed in detail in Section "Theoretical and numerical investigations of parameters affecting reflection". Section "Evaluation of the pipe deformation: FE and physical experiment studies" presents a comprehensive investigation into realistic deformation cases using detailed FE model in conjunction with physical experiment. Two deformation parameters are proposed to evaluate the deformation degree and identify the deformation type. Finally, the main conclusions are given in Section "Conclusions".

Mode characteristics and frequency range of guided waves

Compared with the bulk wave, the guided wave has the characteristics of dispersion and multi-modes, which increase the difficulty of interpretation (Lowe and Cawley 2006). However, if the complexity of guided waves is properly utilized, it can provide more information about the defect (Sun et al. 2018). Therefore, the choice of the excitation mode and frequency is critical for pipe inspection with guided waves. The properties of guided wave propagation and interaction with defects are complex, so the inspection parameters must be carefully selected. The dispersion curve is a crucial tool for selecting the appropriate excitation frequency. Fig. 1 shows a representative dispersion curve for different modes of the pipe used in this paper, drawn according to Gazis' theory (Gazis 1959).

L(0,2) and T (0,1) are the two most widely used modes for practical inspection because they have almost no dispersion in the frequency range of interest, require simple excitation conditions, and possess good sensitivity to full-cross-sectional damage and enables a long-distance inspection capability. Besides, T(0,1) mode is entirely free of dispersion and its tangential displacement is insensitive to non-viscous fluid, so it is suitable for fluid pipeline damage detection (Lowe and Cawley 2006). Therefore, in this paper, L(0,2) and T(0,1) modes are selected for pipeline deformation inspection.

When a symmetric mode guided wave interacts with an axisymmetric damage, only the symmetric mode is reflected in the frequency range. For example, when L(0,2) interacts a symmetric defect, L(0,1) and L(0,2) guided waves will be generated, whereas T(0,1) guided waves will only reflect T(0,1) guided waves at the cutoff frequency of T(0,2). This feature helps simplify the study of reflectivity. When a symmetric mode guided wave interacts non-axisymmetric damage, the mode conversion will occur, resulting in a nonsymmetric flexural mode. Therefore, the reflected flexural mode is an essential basis for judging whether there is a non-axisymmetric defect. Researchers have carried out a series of studies on this (Demma et al. 2003; Lowe et al. 1998) and established the commonly used incident wave mode conversion rules. Namely, L(0,1), T(0,1), L(0,2) are usually converted to F(1,1), F(2,1), …, F(1,2), F(2,2), …, F(1,3), F(2,3), …. With an increase in the incident wave frequency, there will be more corresponding high-order flexural modes.

Fig. 2(a), (c) show representative mode shapes of the T(0,1) and L(0,2) modes. It can be seen that the tangential displacements and axial displacement are approximately constant through the thickness (green line in Fig. 2(a) and red line in Fig. 2(c)). The F(1,2) mode is converted from T(0,1) mode, and both axial and radial components can be seen in Fig. 2(b). The F(1,3) mode is converted from L(0,2) mode, and the tangential component can be seen in Fig. 2(d).

Finite element modeling

FE models have been successfully applied to simulate the interaction of ultrasonic guided waves in various types of structural discontinuity defeats in pipes (Moreau et al. 2012; Benmeddour et al. 2011). This paper creates a series of 3D models to study the interaction between the L(0,2) and T(0,1) modes and the deformation in pipes. The modeled pipes are 3-inch nominal bore schedule 40 pipes, with an outer diameter of 88.9 mm, and wall thickness of 5.5 mm. A 3-cycle Hanning window modulated tone burst with a center frequency of 50 kHz is used in the excitation signal. L(0,2) and T(0,1) modes are excited by imposing the displacement profile at one pipe end around the circumference. Specifically, excitation of L(0,2) mode by applying axial displacement load to the nodes, excitation of T(0,1) mode by applying circumferential displacement load to the nodes, as shown in Fig. 4 (c) and (d). The positions of the receiver and defect deformation location are chosen so that the reflected signals from the deformation could be well separated from incident signals and reflected signals from the pipe end, as shown in Fig. 3. A mesh of 8-node hexahedral linear reduced integral element is used. For the whole model, 800 elements along the length, 48 elements around the circumference and 3 elements along the thickness are used, and this results in each element being about 1.5 mm in the axial direction and 4mm in circumference direction. Accordingly, an iteration step time of 5e-8 s is used based on the stability criterion for explicit time integration analysis, as follows:

$$L < \frac{\lambda}{8} \tag{1}$$

$$\Delta T < 0.8 \times \frac{L}{V_g} \tag{2}$$

where L is the element length, λ is the wave length, V_g is the group velocity. ΔT is the iteration step time.

Axisymmetric finite element modeling

Two axisymmetric deformation patterns are simulated using the FE model to analyze the scattering effect of guided waves and deformed cross-sections. As shown in Fig. 4(a), the arc slope model is used to analyze the scattering behavior when the radius changes gradually. The complete deformation model, shown in Fig. 4(b), is used to analyze the overall influence of the front and rear arc slope on the reflection. The deformation shape is set as an arc shape to be close to the actual pipe deformation situation.

Arc slope models

The arc slope model is used to analyze the effect of gradual cross-section change in the reflection of guided waves. The change of section radius simulates the section deformation, and the change in radius is uniform on the cross-section at the same axial position. Both bulge cases in which the radius increases and decreases, respectively, as shown in Fig. 5, are modeled, and these correspond to the front and rear sections of the complete deformation model shown in Fig. 5(d). The arc slope model is modeled by creating two radius regions that are joined by an arc slope. The introduction and variation of the fillets of the connecting part have little effect on the reflection phenomenon. Therefore, we used the simplest straight line to represent the shape at the deformation. The pipe length is set to be 1.2 m with an arc region of 0.7 m from the excitation end of the pipe.

Fig. 6(a) and (b) show the signals received for bulge-up and bulge-down cases. Only one reflected signal is seen in each case followed by the T(0,1) incident wave, which is reflected from the start of the arc. No reflection of the incident wave occurs at the other end of the slope. The amplitude and phase of the reflected wave are almost the same in both cases. It can be concluded that reflection occurs at the location of severe deformation, and no further reflection takes place in the subsequent gradual deformation region.

Fig. 6(c) shows the received signal for the dent case (Fig. 5(c)). From Fig. 6(a) and Fig. 6(c), it can be seen that although the deformation directions are different (actually opposite), the reflectivity (magnitude of the reflection) of the guided waves is almost the same. This observation suggests that the direction of deformation is not a factor affecting reflectivity.

From Fig. 6, it can also be observed that when the guided wave interacts with a deformed position with a larger radius, the reflected guided wave is in phase with the incident wave. When the guided wave interacts with a deformed position with a smaller radius, the reflected guided wave is out of phase with the incident wave. This rule may provide a basis for determining the direction of deformation.

The reflection coefficient (RC) is defined as the ratio of the reflected signal from the defect to that of the incident signal, and is calculated in the frequency domain. RC is an index that can be used to judge the severity of the defect. Fig. 7 shows the RC spectra of the T(0,1) mode and L(0,2) mode from arc steps with 20% and 50% maximum radial change, plotted against the ratio of the axial extent of deformation (L) to the wavelength (λ). It can be seen that L(0,2) and T(0,1) have the same trend, and the reflection amplitude of L(0,2) is higher than T(0,1). When L/λ is less than 70%, the RC decreases significantly with the increase of L/λ, and then the trend of decrease tends to be smooth until almost a constant value.

It can be concluded that the reflectivity is related to the maximum degree of deformation at the cross-section and the axial extent of the deformation. For the same maximum cross-sectional deformation, the reflectivity decreases with the increase of the deformation range in the axial direction. Conversely, the reflectivity increases for the same axial range as the maximum degree of the cross-sectional deformation increases. Therefore, it can be inferred that the rate of change of cross-sectional deformation with the axial direction, $\Delta R/L$, determines the RC.

Arc deformation models

To simulate the arc deformation of the pipeline shown in Fig. 5(d), a complete deformation model is used to analyze the overall influence of the front and rear arc slope on the reflection. The deformation shape is set to an arc shape to resemble the actual pipe deformation situation closely. It can be deduced from the observations made in Section "Arc slope models" that when a guided wave interacts a complete axisymmetric deformation section, two waves will be reflected, from the front and rear sections of the deformation, respectively. Using the superposition method, the total RC of the deformation is obtained as

$$RC = R_f + R_r e^{i(\Delta\phi)} \tag{3}$$

where R_f and R_r are the RC modulus of the front and the rear reflections from the deformation, $\Delta\phi$ is the phase difference between the waves reflected from the two end sections of the deformation, given by

$$\Delta\phi = 2kL = \frac{4\pi L}{\lambda} \tag{4}$$

The two waves interact destructively when $\Delta\phi=(2n+1)\pi$ and constructively when $\Delta\phi=2m\pi$, where, n and m are integers.

Fig. 8 shows the RC spectrum from bulge deformation with 22.5% maximum radial change. When L/λ is below 70%, RC decreases sharply as L/λ increases. This may be explained by referring to Fig. 7, from which it can be seen that when L/λ is below 70%, the RC of the reflection of the arc step decreases rapidly as the L/λ increases. Therefore, the behavior of the overall RC is dominated by the axial extent of the deformation in this range, such that as L increases, the deformation rate decreases. When L/λ exceeds 70%, however, RC oscillates periodically due to interaction between two waves from the two end sections of the deformation, and the amplitude tends to decrease smoothly. It can also be observed that at $L/\lambda=75\%$, 125%, and 175%, the minima of the RC occur, and at $L/\lambda=100\%$ and 150%, the maxima occur. The maxima of the RC occur at $L/\lambda=\eta/2$ and the minima occur at $L/\lambda=(2\eta-1)/4$, where η is an integer. This is different from the reflection characteristic in the case of a notch, because the phase difference from two reflected waves of the deformation are not out of phase like what happens at a notch.

Non-axisymmetric finite element modelling

When axisymmetric guided waves interact with non-axisymmetric damage, the waveform mode conversion will occur. Non-axisymmetric FE deformation models can be used to study the deformation parameters that affect the mode conversion. In this section, 3D non-axisymmetric dent models are created to study the influence of deformation parameters on reflection and mode conversion. Fig. 9 shows a representative FE model and the parameters defining the dent deformation.

Fig. 10 shows the signal of L(0,2) mode and F(1,3) mode. There is no phase delay in the displacements at different angles on the circumference for axisymmetric modes when the symmetric mode guided wave is excited. For the reflection of the symmetric mode, the individual signals from the nodes are superposed. The resulting signal is the total reflection of the symmetric mode. For the reflection of the F(n, m) mode, the phase delay at each position on the circumference is determined by $n\theta/2\pi$, where n is the circumferential order number, θ is the angular distance from the center of the defect (Hayashi and Murase 2005). Therefore, a phase delay of $n\theta/2\pi$ is added to each signal before adding them.

The relationship between RC of F(1,3) and the axial deformation range under a certain deformation depth has been investigated to analyze the deformation parameters that affect the mode conversion. Fig. 11 shows the RC spectra of the F(1,3) mode from arc steps with 33% and 66% maximum radial change versus the circumferential extent of the deformation. It can be seen that the

RC increases with maximum radial change and decreases with circumferential extent. When the circumferential extent is below 20% of the circumference, the RC of F(1,3) decreases sharply, and the decrease becomes smooth as the circumferential extent exceeds 20%. Besides, the absolute values of RC are different under the two cases, and is much larger under the 66% maximum radial change. Therefore, it can be inferred that the rate of change of cross-sectional deformation concerning the circumferential direction determines the RC of F(1,3).

Theoretical and numerical investigations of parameters affecting reflection

Relationship between reflection coefficient and deformation parameters

Fig. 12 shows snapshots of the L(0,2) mode incident wave propagating along the pipe and interacting at the deformation from the FE simulation. It can be seen that when the guided wave interacts with the deformed region, most of the energy is transmitted and a few of it is reflected back, and the guided wave mode does not change.

Referring back to Fig. 6, where the RC spectra of the L(0,2) and T(0,1) modes from arc steps with 20% and 50% maximum radial change versus the axial extent of deformation to the wavelength have been shown. From the results, it is reasonable to consider L and ΔR as two key parameters affecting the RC, and RC tends to be equal in the case of the same ratio of $\Delta R / L$.

A simplified deformation model is proposed herein for an axisymmetric deformation case, as shown schematically in Fig. 13. For generality, the deformation model includes two pipes of the same size, connected by an arc section. The axial extent of $2L$ is assumed to be long enough so as to separate the reflections from the start and the end sections of the deformation. Due to the deformation of the section, the traditional plate theory cannot be applied. Considering longitudinal mode guided waves have a high similarity to acoustic waves in fluids, because they manifest as axial displacement. Therefore, we used acoustic energy method in fluid medium instead to simplify the derivation of the reflection coefficient.

Consider a sufficiently small volume element in the sound field, whose original volume is V_0, pressure is P_0, density is ρ_0, and velocity is v. The kinetic energy ΔE_k obtained by the volume element due to acoustic perturbation is (Kinsler et al 2000):

$$\Delta E_k = \frac{1}{2}(\rho_0 V_0)\ v^2 \tag{5}$$

In addition, due to the acoustic perturbation, the volume element pressure increases from P_0 to $P_0 + P$, the volume changes from V_0 to V, so that the volume element has potential energy ΔE_p:

$$\Delta E_p = -\int_{v_0}^{v} p dV \tag{6}$$

$$dp = c_0^2 d\rho^{'} \tag{7}$$

Eq. (7) describes the relationship between the slight change of pressure intensity dp and the small density change $d\rho$. For small-amplitude waves, c_0 is approximately a constant (Kim 2010).

Considering that the mass of the volume element remains constant during compression and expansion, there is a relationship between the change in volume of the volume element and the change in density:

$$dp = -\frac{\rho_0 {c_0}^2}{V_0} dV \tag{8}$$

Substituting Eq. (8) into Eq. (6):

$$\Delta E_p = \frac{V_0}{\rho_0 {c_0}^2} \int_{\rho_0}^{\rho} {c_0}^2 (\rho - \rho_0) \frac{V_0}{\rho_0} d\rho = \frac{V_0}{2\rho_0 {c_0}^2} p^2 \tag{9}$$

$$\Delta E = \Delta E_k + \Delta E_p = \frac{V_0}{2} \rho_0 (v^2 + \frac{1}{{\rho_0}^2 {c_0}^2} p^2) \tag{10}$$

Eq. (10) represents the instantaneous value of the wave energy in the volume element, and if it is averaged over a period, the time average of the wave energy $\overline{\Delta E}$ is obtained as:

$$\overline{\Delta E} = \frac{1}{T}\int_0^T \Delta E dt = \frac{1}{2} V_0 \frac{{p_0}^2}{\rho_0 {c_0}^2} \tag{11}$$

The average wave energy in a unit volume is called the average sound energy density I, i.e.,

$$I = \frac{\Delta E}{V_0} = \frac{{p_a}^2}{2\rho_0 {c_0}^2} \tag{12}$$

According to the energy relationship of the guided wave passing through the interface, the reflection coefficient r_I and transmission coefficient t_I are:

$$r_I = \frac{I_r}{I_i} = \frac{|p_{ra}|^2}{2\rho_1 c_1} / \frac{|p_{ia}|^2}{2\rho_1 c_1} = \left(\frac{R_2 - R_1}{R_2 + R_1}\right)^2 = \left(\frac{R_{12} - 1}{R_{12} + 1}\right)^2 \tag{13}$$

$$t_I = \frac{I_t}{I_i} = \frac{|p_{ia}|^2}{2\rho_2 c_2} / \frac{|p_{ia}|^2}{2\rho_1 c_1} = 1 - r_I = \frac{4R_{12}}{(1+R_{12})^2} \tag{14}$$

where R_1 and R_2 denote the acoustic impedance of the two media, and $R_{12}=R_1/R_2$. Since the material at the deformation interface is uniform, the cross-section will affect the acoustic impedance. If we consider that the axial displacement is almost constant through the thickness and that the radius of the pipe is much bigger than the thickness, we can approximate the value of the reflection coefficient obtained at a step in a pipe by using the formula:

$$R_{12} = \frac{A_2}{A_1} \tag{15}$$

where A_1 and A_2 are the cross-section area before the deformation part and after the deformation part, corresponding to the AB and AC, respectively, in Fig. 14.

From the geometric relationship, it can be deduced that：

$$A_1 = d \tag{16}$$

$$A_2 = A_1 \cdot \sin(\pi / 2 - 2 * \alpha) \tag{17}$$

$$\beta = \frac{A_2}{A_1} \tag{18}$$

$$r_l = \frac{(\beta-1)^2}{(\beta+1)^2} \tag{19}$$

The analytical and FEM simulation results are shown in Fig. 14. As can be seen, the numerical results are in good agreement with the theoretical predictions, especially for relatively high detection frequencies. The results verify the rationality of Eqs. (16)-(19) and the proposed model, and as the frequency increases, the numerical results gradually approach the analytical solution. This is because the theoretical formula is derived from an energy perspective and does not consider the dynamic/frequency effect on reflectivity. For the same detection frequency, the guided wave reflection coefficient increases monotonically with the increase of the deformation rate. The detection frequency also affects the reflection coefficient of the deformed echo. The reflection coefficient decreases with the increase of the detection frequency overall, and the frequency effect is more obvious in the lower frequency range.

Relationship between mode conversion with deformation parameters

As shown in Fig. 11, the RC spectra of the F(1,3) mode from non-axisymmetric deformation with 33% and 66% maximum radial change vary with the circumferential extent of deformation. This suggests that C and ΔR can be considered as two key parameters affecting the mode conversion.

To understand more quantitatively as how these parameters affect the mode conversion, the effect of the deformation depth is investigated by varying the deformation depth for a fixed deformation angle and deformation axial extent. Similarly, the effect of deformation angle on the mode conversion is investigated by varying the deformation depth for a fixed deformation depth and deformation axial extent.

Fig. 15(a) shows the variation of mode conversion with the deformation depth at two specific deformation angles of 45º and 60º, respectively. It can be seen that, for the same deformation circumferential angle, the guided wave mode conversion ratio of (L(0,2) to F(1,3)) basically remains the same with the increase of the deformation depth. The overall amplitude at 60º circumferential angle is lower than that at 45º.

Fig. 15(b) shows the variation of mode conversion with the deformation angle at two given deformation depths of 5mm and 6.7mm, respectively. It can be seen that, for the same deformation depth, the guided wave mode conversion ratio of (L(0,2) to F(1,3)) decreases monotonically with the increase of the deformation angle. This means that, while the mode conversion ratio is little affected by the deformation depth, it is affected markedly by the deformation circumferential extent. As the deformation circumferential angle increases, the mode conversion ratio decreases. Therefore, the mode conversion ratio may be regarded as a parameter for judging the degree of deformation concentration.

According to the theory of guided wave propagation (Rose 2014), the displacement at any point on a hollow cylinder is formed by the superposition of guided waves of n modes (Murase et al. 2005).

$$u(r,\theta,z,t)=\sum_{n=-\infty}^{+\infty}\sum_{m=1}^{+\infty}A_{nm}(\omega)N_{nm}(r)\exp(in\theta+ik_{nm}z-i\omega t) \qquad (20)$$

where integer n denotes the circumferential order, $N_{nm}(r)$, $A_{nm}(\omega)$ are the function of the displacement distribution in the thickness direction and amplitude for the *m*th mode in the *n*th family, respectively, and k_{nm} is the wave number.

L(0,2) mode at relatively low frequencies (⩽300 kHz) is commonly used because of its high speed. This frequency range is usually below the cutoff frequency of the L(n,3) mode group; therefore, for excitation at L(0,2) mode, there mainly exists L(0,2) mode in a pipe, and consequently Eq. (20) can be simplified to:

$$u(\theta, z, t) = \sum_{n=-\infty}^{+\infty} A_n(\omega)\exp(in\theta + ik_n z - i\omega t) \tag{21}$$

In actual situations, the number of receiving sensors is finite. Assuming N receiving positions in the circumferential direction at regular intervals θ_0,

$$\theta_0 = \frac{2\pi}{N} \tag{22}$$

$$\theta_k = \frac{2\pi}{N}(k-1) \tag{23}$$

Then the received displacement signals at $\theta = \theta_k$, $Z = Z_R$ are:

$$u^R(\theta_k, z_R, t) = \int_{\theta_k-\theta_0/2}^{\theta_k+\theta_0/2} u(\theta_k, z_R, t) r_0 d\theta = r_0 \sum_{n=-\infty}^{+\infty} A_n(\omega) f_n(\theta_0)\exp(in\theta_k + ik_n z_R - i\omega t) \tag{24}$$

where r_0 is the outer diameter of the pipe, and

$$f_n(\theta_0) = \begin{cases} \theta_0, n = 0 \\ \dfrac{2\sin(n\theta_0/2)}{n}, n \neq 0 \end{cases} \tag{25}$$

There is no phase delay in the displacement of different nodes on the same circle for an axisymmetric mode. But for a flexural mode, the phase delay is determined by $n\theta/2\pi$, where n is the circumferential order and θ is the circumferential angle between the two nodes when taking the node on the same axis as the center of the defect as the reference point. Compensate $n\theta/2\pi$ for the tangential displacement of each node in the circumferential direction, and superimpose the compensated signals, the corresponding *n*th order bending mode signal can be obtained. In other words, by multiplying a weight function of $\exp(-in_E\theta_k)$, the multi-mode guided wave can be separated. The displacement corresponding to the extracted *n*th order mode at $\theta=\theta_k$, $z=z_R$ is:

$$u_{n_E}^{ext}(\theta_k, z_R, t) = r_0 \sum_{n=-\infty}^{+\infty} A_n(\omega) f_n(\theta_0) \exp(i(n-n_E)\theta_k + ik_n(\omega)z_R - i\omega t) \tag{26}$$

Summing with respect to k gives

$$u_{n_E}^{ext}(z_R, t) = r_0 \sum_{k=1}^{N} u_{n_E}^{ext}(\theta_k, z_R, t) \approx r_0 A_n(\omega) f_n(\theta_0) \exp(ik_n(\omega)z_R - i\omega t) \tag{27}$$

The extracted signal is shown in Fig. 10(b) previously is of the first-order flexural mode. Since the excitation signal is entirely symmetrical, the component of the excitation guided wave is almost invisible in the flexural mode signal. When a symmetrical guided wave interacts with a local deformation defect, a non-axisymmetric guided wave will be reflected, and its displacement distribution over the circumference is no longer a symmetrical circle. After the asymmetric part is superimposed, a flexural mode guided wave is generated. Since the symmetrical point about the center of the circle has a phase compensation difference of π, the phase of the symmetrical guided wave received by the symmetrical point is basically the same, so the symmetrical point has a negative phase relationship after phase compensation. Therefore, Eq. (27) can be re-written as

$$\begin{aligned}
u_{n_E}^{ext}(z_R, t) &= r_0 \sum_{L=1}^{N/2} u_L^{ext}(\theta_L, z_R, t) + u_L^{ext}(\theta_{L+N/2}, z_R, t) \\
&= r_0 f_n(\theta_0) \exp(i(k_n(\omega)z_R - \omega t) \sum_{L=1}^{n/2} (A_L(\omega)\exp(i(n-n_E)\theta_k + A_{L+N/2}\exp(i(n-n_E)\theta_{k+\pi}) \\
&= r_0 f_n(\theta_0) \sum_{L=1}^{N/2} u_L^{ext}(\theta_L, z_R, t) + u_L^{ext}(\theta_{L+N/2}, z_R, t) \\
&= r_0 f_n(\theta_0) \sum_{L=1}^{N/2} A_L(\omega) - A_{L+N/2}(\omega)
\end{aligned} \tag{28}$$

Eq. (28) shows that the circumferential displacement distribution affects the amplitude of the guided wave in the flexural mode. The more asymmetrical the displacement circumferential distribution is about the circle's center, the larger the flexural mode signal will be.

Fig. 16 shows the circumferential distribution of the reflected displacement received under different circumferential deformation extent. It can be seen that, as the circumferential deformation extent increases, the overall amplitude of the displacement circumferential distribution does not change significantly, while the symmetry for the center of the circle gradually increases. On the other hand, as the deformation depth increases, the symmetry for the center of the circle does not change significantly, whereas the overall amplitude of the displacement gradually increases. This explains the phenomenon observed in Fig. 15 that the mode conversion decreases with the increase of the circumferential deformation extent.

Evaluation of the pipe deformation: FE and physical experiment studies

This section presents a more realistic deformation case study, using FE simulation in conjunction with experimental validation.

FE predictions

To study the effects of different types of pipe deformations on the guided wave reflection, both overall section deformation and local section deformation are considered here. Fig. 17 depicts the fabrication processes to simulate the local and overall deformations in two pipes. For the sake of convenience in manufacturing the cross-sectional geometry of the deformation, two identical steel pipes with an outer diameter of 20 mm, a wall thickness of 1 mm and length of 500 mm are chosen for the experiment, and the same dimensions are used in the FE simulation.

In Fig. 17(a), the pipe is fixed on a rigid plate, and a hammer head is pressed perpendicular to the circumferential surface of the pipe. The contact part of the hammer head is hemispherical of diameter 8 mm. In Fig. 17(b), the pipe is also fixed on a rigid plate, and a steel bar (length 80mm, diameter 8mm) is pressed tangent to the circumferential surface of the pipe. Thus, it is possible to increase the same depth of both dents with this setup by continuously applying a displacement load.

Fig. 18 shows the FE computed variation of L(0,2) and F(1,3) reflection coefficients at a frequency of 230 kHz with the dent depth, for the two deformation types respectively. It can be seen that the L(0,2) and F(1,3) reflection coefficients from a local deformation are essentially linear functions with the dent depth. The L(0,2) and F(1,3) reflection coefficients from an overall deformation also approximate a linear function with the dent depth. As the depth increases beyond half of the radius, the increase in the reflection coefficients tends to ease.

Comparing the reflection coefficients from the two deformation types, it can be observed that the L(0,2) reflection coefficient from the overall deformation is higher than that from the local deformation. This may be explained by the nature of the overall deformation, which leads to more cross-sectional area deformation, causing higher deformation severity. Meanwhile, the F(1,3) reflection coefficients from both types of the pipe deformation are almost identical, which means that the mode conversion rate from L(0,2) to F(1,3) from a local dent is higher than from an overall dent. This is also consistent with the conclusion in Section "Relationship between mode conversion with deformation parameters" that the mode conversion rate decreases with the increase of the circumferential extent of deformation. The mode conversion rate from overall deformation is higher than that from the local deformation.

Therefore, a single deformation parameter by a dent depth cannot sufficiently reveal the relationship between the deformation and the RC and mode conversion.

Experimental validation

A physical experiment was conducted to validate the theoretical and FE predictions. In the experiment, the pipe deformation was fabricated by a multipurpose servo-hydraulic universal testing machine, using the displacement control mode to create the desired deformation. A hammer formed the local deformation with a semi-circular head, and the overall deformation was formed by a steel bar, as illustrated in Fig. 19(a). With this setup, it was possible to increase the depth of both dents by applying successive distributive forces and obtain the ideal deformation case. Fig. 19(b) shows typical profiles for the two types of deformation.

The experimental pipes were made of steel pipes with an outer diameter of 20 mm and wall thickness of 1 mm. Fig. 20 shows the setup for the guided wave experiment on the test pipes. During the test, the pipe was placed horizontally on a polyethylene foam sheet, from which the reflection can be negligible. The excitation signal was a 5-cycle Hanning window modulated tone burst generated by an arbitrary function generator (Tektronix AFG3022) and amplified by a high-voltage power amplifier (Pintech HA-205). The reflection signal was collected by a digital oscilloscope (RTB-2002).

PZT transducers did the signal excitation and reception. 8 rectangle PZT transducers were used for the excitation and reception. These transducers are 12mm long and 4mm wide, and they were attached at equal intervals around the pipe wall. Due to the axial vibration from the transducer face and the frequency selection, L(0,2) mode was the dominant mode that was generated. The reflected L(0,2) mode wave was received by a transducer ring comprised of 8 rectangle PZTs.

Fig. 21 shows the comparison between FE predictions and experimental results for both deformation cases. It should be noted that when the deformation depth is less than 4 mm, the reflected signal was submerged in the noise and therefore was not measured. After the deformation reaches 4mm, good agreement between the FE predictions and tests results can be observed. The small difference in the amplitude of the reflection is probably due to the attenuation effect which is not simulated in the FE model but exists in the actual experiment.

Characterization of the pipe deformation ratio

Due to the complexity of pipeline cross-sectional deformation in practice, using parameters in one direction cannot sufficiently characterize the actual deformation. However, from the results under an axisymmetric deformation, it can be postulated that the reflectivity of the guided wave is positively correlated with the rate of change of the deformation. Thus, we propose a quantitative parameter, called axial deformation severity rate δ, to characterize the deformation severity extent in the axial direction, and similarly a circumferential deformation rate β to characterize the deformation severity extent in the circumferential direction. The two severity parameters are defined as:

$$\delta=\frac{\left|D_{\max}-D\right|+\left|D-D_{\min}\right|}{L} \tag{29}$$

$$\beta=\frac{D_{\max}-D_{\min}}{D_{\max}+D_{\min}} \tag{30}$$

Where, $D_{\max}$ and $D_{\min}$ are the maximum and minimum diameters after deformation. L is the length of the deformation zone in the axial direction. Tables 1 and 2 list the geometric parameters of each test pipe with different degrees of local and overall deformations, along with the deformation severity parameters calculated from the above equations. The relationship between the parameters δ, β and the reflection coefficient of the reflected signals is analyzed.

Fig. 22 shows the correlation between the deformation parameter δ , β and the deformation depth under the two types of deformation. It can be seen that the δ and β from both types of dents are approximately linearly related to the dent depth. The values of δ under an overall deformation dent are higher than that under a local deformation dent, which is due to a greater change in the cross-sectional area under an overall deformation. In general, the parameter δ and β reflects well the degree of deformation.

Fig. 23 and 24 show the L(0,2) and F(1,3) varying with the deformation parameters δ and β from the experiment results. It can be observed that the parameters δ, β are well correlated with RC of L(0,2) and F(1,3). The RC of L(0,2) and F(1,3) are approximately a linear function with δ, β respectively in two types of the dent deformation. Moreover, the ratio $\gamma = \delta / \beta$ represents the degree of deformation concentration and its relationship with the mode conversion ratio curve can be used to judge the deformation type, as can be seen in Fig. 25. The amplitude of the mode conversion from a local deformation is significantly higher than that from an overall deformation.

$$\gamma = \delta / \beta = \frac{D_{\max} + D_{\min}}{L} \tag{31}$$

Conclusions

A quantitative study of the reflection of the guided wave from cross-sectional deformation in pipes has been carried out, using finite element modelling and experimental validation. A practical method of estimating the severity and the type of deformation has been proposed based on the relationship established from the numerical and experimental studies.

Based on the results, the following conclusions can be drawn.

1) The reflection occurs at the start of the cross-sectional deformation, while the subsequent gradual deformation region does not cause reflection. The RC from an arc slope is dependent on the maximum radial change and axial length of the slope. In conjunction with a theoretical analysis using the wave energy theory, the RC can be regarded as an effective index to judge the severity of the deformation.

2) The superposition approach can be applied to reconstruct the reflection coefficient of a deformation region by using the reflection and transmission characteristics of the slope up and slope down part. The RC oscillates periodically due to interaction between two waves from the two end sections of the deformation

3) The mode conversion ratio is rarely affected by the deformation depth, but is affected by the deformation circumferential extent. As the deformation circumferential angle increases, the mode conversion ratio decreases.

4) The FE simulation and experimental validation have been used to evaluate the deformation by guided waves for real deformation cases. Two quantitative parameters, namely an axial deformation severity degree and a circumferential deformation severity degree, are defined. For both types of deformation, it has been shown that the reflection coefficients of the L(0,2) and F(1,3) modes are approximately a linear function of axial δ and β respectively, whereas the mode conversion ratio (L(0,2) to F(1,3)) are linearly related with the circumferential deformation rate δ / β and can be used to judge the deformation type.

It should be noted that the environmental variations on damage detection are not considered in this paper. Further studies will be needed for more complex deformation geometries and real monitoring situations. The reflection phenomenon difference between shape deformation and notch type of defects will also be studied.

Data Availability Statement

All data, models, and code generated or used during the study appear in the submitted article.

Acknowledgements

This study was financially supported by National Program on Key Research and Development Project of China (2020YFB2103502), National Science Fund for Distinguished Young Scholars of China (51625803), Program of Chang Jiang Scholars of Ministry of Education, the support from the Tencent Foundation through the XPLORER. These supports are gratefully acknowledged.

References

Alleyne, D. N., Pavlakovic, B., Lowe, M. J. S., and Cawley, P. (2004). “Rapid, long range inspection of chemical plant pipework using guided waves.” *Key Eng. Mat.* 270-2073 (1): 434-441. https://doi.org/10.4028/www.scientific.net/KEM.270-273.434

Benmeddour, F., Treyssède, F., and Laguerre, L. (2011). “Numerical modeling of guided wave interaction with non-axisymmetric cracks in elastic cylinders.” *Int. J. Solids Struct.* 48: 764–774. https://doi.org/10.1016/j.ijsolstr.2010.11.013.

Carandente, R., Ma, J., and Cawley, P. (2010). “The scattering of the fundamental torsional mode from axi-symmetric defects with varying depth profile in pipes.” *J. Acoust. Soc. Am.* 127: 3440–3448. https://doi.org/10.1121/1.3373406.

Carandente, R., and Cawley, P. (2012). “The effect of complex defect profiles on the reflection of the fundamental torsional mode in pipes.” *NDT E Int.* 46: 41–47. https://doi.org/10.1016/j.ndteint. 2011.11.003.

Demma, A., Cawley, P., Lowe, M., and Pavlakovic, B. (2005). “The effect of bends on the propagation of guided waves in pipes.” *J. Pressure vessel Technol.* 127(3): 328-335. https://doi.org/10.1115/1.1 990211

Demma, A. (2001). “Mode conversion of longitudinal and torsional guided modes due to pipe bends.” American Institute of Physics. 557:172-179. https://doi.org/10.1063/1.1373756.

Demma, A., Cawley, P., and Lowe, M. (2003). “The reflection of the fundamental torsional mode from cracks and notches in pipes.” *J. Acoust. Soc. Am.* 114: 611–625. https://doi.org/10.1121/1.158 2439.

Demma, A., Cawey, P., and Lowe, M. (2004). “The reflection of guided waves from notches in pipes: a guide for interpreting corrosion measurements.” *NDT E Int.* 37: 167–180. https://doi.org/10.1016/j.ndteint.2003.09.004.

Duran, O., Althoefer, K., and Seneviratne, L. D. (2003). “Pipe inspection using a laser-based transducer and automated analysis techniques.” *IEEE-Asme T Mech.* 8 (3): 401-409. https://doi.org/10.1109/TMECH.2003.816809

Gazis, D. C. (1959). “Three-dimensional investigation of the propagation of waves in hollow circular cylinders. i. analytical foundation.” *J. Acoust. Soc. Am.* 31(5): 568-573. https://doi.org/10.1121/1.1907753

Gazis, D. C. (1959). “Three-dimensional investigation of the propagation of waves in hollow circular cylinders. ii. numerical results.” *J. Acoust. Soc. Am.* 31 (5): 573-578. https://doi.org/10.1121/1.1907754

Ge, T., Xu, Z. D., and Yuan, F. G. (2022). “Predictive model of dynamic mechanical properties of VE damper based on acrylic rubber–graphene oxide composites considering aging damage.” *J. Aerospace Eng.* 35(2): 04021132. https://doi.org/10.1061/(ASCE)AS.1943-5525.0001385

Hayashi, T., Kawashima, K., and Rose, J. L. (2004). “Calculation for guided waves in pipes and rails.” *Key Eng. Mat.* 270-273: 410-415. https://doi.org/10.4028/www.scientific.net/KEM.270-273.410

Hayashi, T., and Murase, M. (2005). “Mode extraction technique for guided waves in a pipe.” *Nondestruct. Test. Eval.* 20: 63–75. https://doi.org/10.1080/10589750500062771.

Hayashi, T., Song, W. J., and Rose, J. L. (2004). “Guided wave dispersion curves for a bar with an arbitrary cross-section, a rod and rail example.” *Ultrasonics*. 41(3):175-183. https://doi.org/10.1016/S0041-624X(03)00097-0

Kim, D. K, Cho, S., H, Seoung, Soo, Park, S. S., Yoo, H. R. (2003). “Development of the caliper system for a geometry pig based on magnetic field analysis.” *J. Mech. Sci. Technol.* 17 (12): 1835-1843. https://doi.org/10.1007/BF02982422

Kim, Y. H. (2010). “Sound Propagation: *An Impedance Based Approach.*” Singapore: Wiley

Kinsler, L. E., Frey, A. R., Coppens, A. B., and Sanders, J. V. (2000). “*Fundamentals of acoustics*.” 4th ed. New York: Wiley

Lam, C., and Zhou, W. (2016). “Statistical analyses of incidents on onshore gas transmission pipelines based on PHMSA database.” *Int. J. Press. Vessel. Pip.* 145: 29–40. https://doi.org/10.1016/j.ijpvp.2016.06.003.

Lovstad, A., and Cawley, P. (2011). “The reflection of the fundamental torsional guided wave from multiple circular holes in pipes.” *NDT E Int.* 44: 553–562. https://doi.org/10.1016/j.ndteint.2011.05.010.

Lovstad, A., and Cawley, P. (2012). “The reflection of the fundamental torsional mode from pit clusters in pipes.” *NDT E Int.* 46: 83–93. https://doi.org/10.1016/j.ndteint.2011.11.006.

Lowe, M., Alleyne, D. N., and Cawley, P. (1998). "The Mode Conversion of a Guided Wave by a Part-Circumferential Notch in a Pipe." *J. Appl. Mech. Trans.* 65(3):649-656. https://doi.org/10.1115/1.2789107.

Lowe, M., and Cawley, P. (2007). "Long Range Guided Wave Inspection Usage – Current Commercial Capabilities and Research Directions. department of mechanical engineering.

Lu, H. F., Xu, Z. D., Iseley, T., and Matthews, J. C. (2021). "A novel data-driven framework for predicting residual strength of corroded pipelines." *J. Pipeline Syst. Eng.* https://doi.org/10.1061/(ASCE)PS. 1949-1204.0000587.

Ma, S., Wu, Z., Wang, Y., and Liu, K. (2015). "The reflection of guided waves from simple dents in pipes." *Ultrasonics*. 57:190-197. https://doi.org/10.1016/j.ultras.2014.11.012

Moreau, L., Velichko, A., and Wilcox, P. D. (2012). "Accurate finite element modelling of guided wave scattering from irregular defects." *NDT E Int.*, 45(1):46-54. https://doi.org/10.1016/j.ndteint.2011.09.003.

Murase, M., Hayashi, T., Nagao, M., and Okuda, Y. (2005). "Mode Extraction and Defect Detection Using a Multi-Channel Array with Magnetostrictive Transducer and Mode Extraction". *Review of Progress in Quantitative Nondestructive Evaluation.* American Institute of Physics.

Na, W. B., and Kundu, T. (2002). "Underwater pipeline inspection using guided waves.". *J. Press. Vessel Technol. Trans.* 124: 196–200. http://doi.org/10.1115/1.1466456

Ni, P., and Mangalathu, S. (2018). "Fragility analysis of gray iron pipelines subjected to tunneling induced ground settlement." *Tunn. Undergr. Sp. Technol.* 76: 133–144. https://doi.org/10.1016/j.tust.2018.03.014.

Rose, J. L. (2014). "Ultrasonic Guided Waves in Solid Media: Plates." Cambridge University Press.

Shan, K., Shuai, J., Xu, K., Zheng, W. (2018). "Failure probability assessment of gas transmission pipelines based on historical failure-related data and modification factors." *J. Nat. Gas Sci. Eng.* 52: 356–366. https://doi.org/10.1016/j.jngse.2018.01.049.

Sun, Z., Sun, A., and Ju, B. F. (2018). "Guided wave imaging of oblique reflecting interfaces in pipes using common-source synthetic focusing." *J. Sound Vib.* 420: 1–20. https://doi.org/10.1016/j.jsv.2018.01.012.

Verma, B., Mishra, T. K., Balasubramaniam, K., and Rajagopal, P. (2014). "Interaction of low-frequency axisymmetric ultrasonic guided waves with bends in pipes of arbitrary bend angle and general bend radius." *Ultrasonics.* 54 (3): 801-808. https://doi.org/10.1016/j.ultras.2013.10.007

Wang, L., and Yuan, F.G. (2005). "Damage identification in a composite plate using prestack reverse-time migration technique." *Struct. Heal. Monit*. 4: 195–211. https://doi.org/10.1177/147592170505 5233.

Wang, S. J., Xu, Z. D., Li, S and Shirley, J. Dyke. (2016). "Safety and Stability of Light-Rail Train Running on Multispan Bridges with Deformation." *J. Bridge Eng.* 06016004-1:7

Xu, Z. D., and Wu Z. S. (2007). "Energy Damage Detection Strategy Based on Strain Responses for Long-Span Bridge Structures." *Eng. Struct.* 29(4): 609-617. https://doi.org/10.1016/j.engstruct.2006.06.004

Xu, Z. D., Liu, M., Wu Z. S., and Zeng, X. (2011). "Energy damage detection strategy based on strain responses for long-span bridge structures." *J. Bridge Eng.* 16(5):162-171. https://doi.org/10.1016/j.engstruct.2006.06.004

Xu, Z. D., Wu, K. Y. (2012). “Damage detection for space truss structures based on strain mode under ambient excitation.” *J. Eng. Mech*. 138(10): 1215-1223. https://doi.org/10.1061/(ASCE)EM.1943-7889.0000426

Xu, Z. D., Zeng, X. and Li, S. (2015). “Damage detection strategy using strain-mode residual trends for bridges.” *J. Comput. Civil Eng*. 29(5): 04014064-1:11. https://doi.org/10.1061/(ASCE)CP.1943-5487.0000371

Xu, Z. D., Li, S., and Zeng, X. (2018). “Distributed Strain Damage Identification Technique for Long-Span Bridges Under Ambient Excitation.” Int. J. Struct. Stab. Dy. 18(11): 1850133-1:22. https://doi.org/10.1142/S021945541850133X

Xu, Z. D., Zhu, C., and Shao, L. W. (2021). “Damage Identification of Pipeline Based on Ultrasonic Guided Wave and Wavelet Denoising.” *J. Pipeline Syst. Eng.* https://doi.org/10.1061/(ASCE)PS.1949-1204.0000600

Zhang, X., Zhou, W., Li, H., and Zhang, Y. (2020). “Guided wave-based bend detection in pipes using in-plane shear piezoelectric wafers. *NDT E Int.* 116:102312. https://doi.org/10.1016/j.ndteint.2020.102312

Table 1 Soil parameters of a section of Shanghai Metro Tunnel

Stratum	Thickness （m）	Unit weight （kN/m^3)	Cohesion (kPa)	internal friction angle （φ）	Coefficient of ground spring
Fill ①$_1$	1.9	18	-	-	-
Sandy silt ②$_{3-1}$	1.9	18.6	5	30.5	20
Sandy silt ②$_{3-2}$	4.2	18.3	5	30.5	20
Sandy silt ②$_{3-3}$	4.7	18.3	4	31.5	20
Silty clay ④	5.3	17	14	12.5	2
Clay ⑤$_{1-1}$	3.8	17.6	15	13.5	2
Clay ⑤$_{1-2}$	8	17.9	15	13.5	2

Table 2 List of numerical simulation cases

No.	Heating curves	Duration	Burial depth	Spalling
A1	HC	4h	shallow	⊗
A2	HC	4h	medium	⊗
A3	HC	4h	deep	⊗
AS1	HC	4h	shallow	☑
AS2	HC	4h	medium	☑
AS3	HC	4h	deep	☑
B1	RABT	4h	shallow	⊗
B2	RABT	4h	medium	⊗
B3	RABT	4h	deep	⊗
BS1	RABT	4h	shallow	☑
BS2	RABT	4h	medium	☑
BS3	RABT	4h	deep	☑

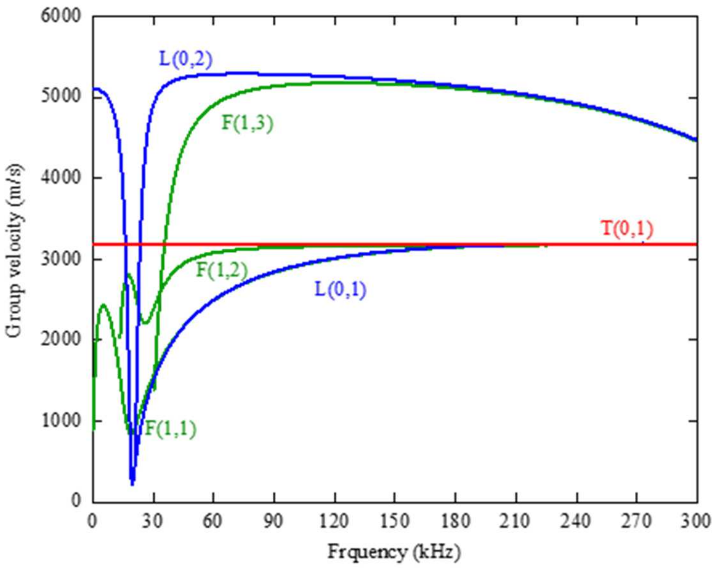

Fig. 1. Group velocity dispersion curves for a steel pipe (outer diameter 88.9mm and wall thickness 5.5mm).

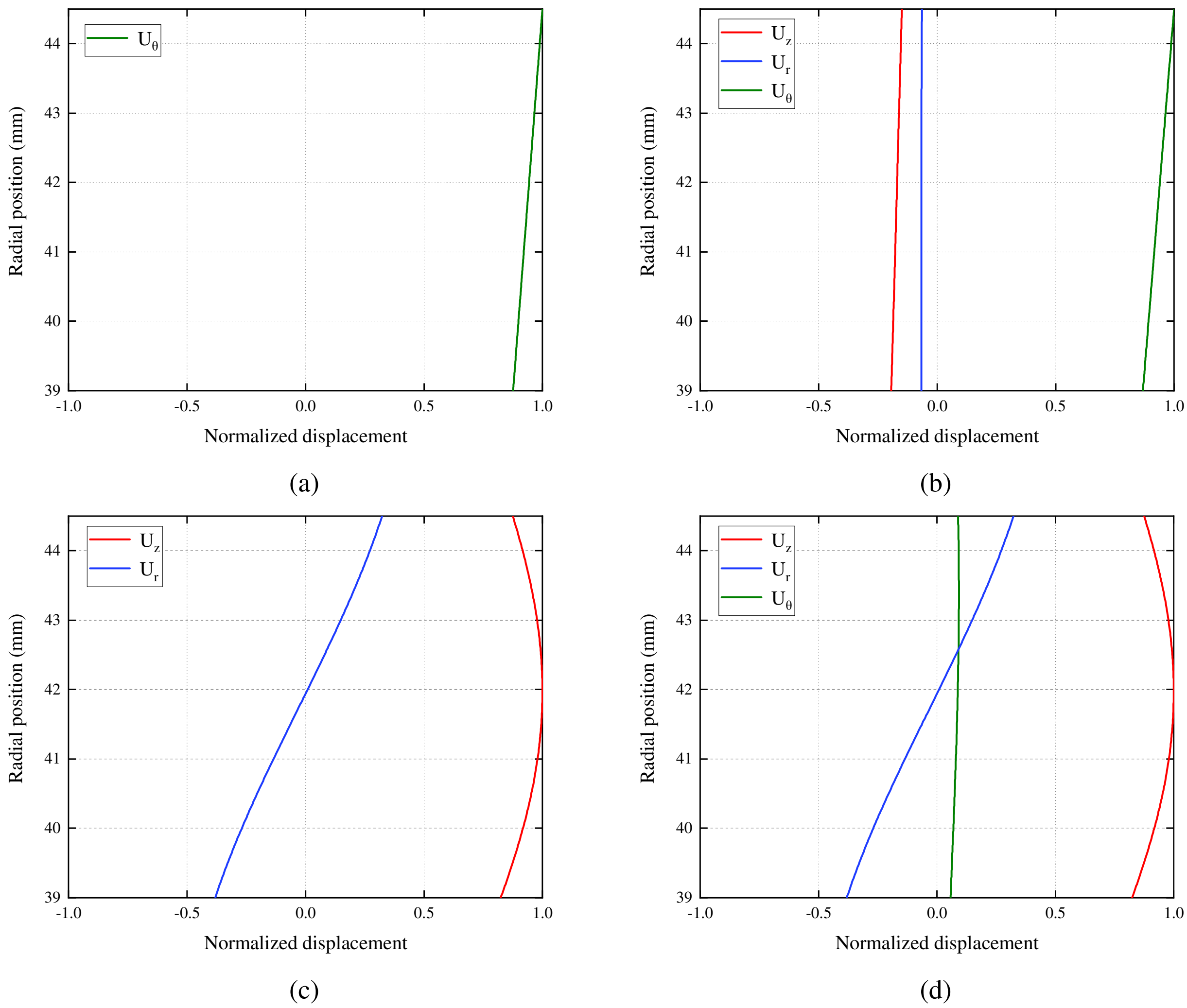

Fig. 2. Displacement mode shapes in a steel pipe (outer diameter 88.9mm and wall thickness 5.5mm) at 50kHz for (a) T(0,1) and (b) F(1,2); 230kHz for (c) L(0,2) and (d) F(1,3).

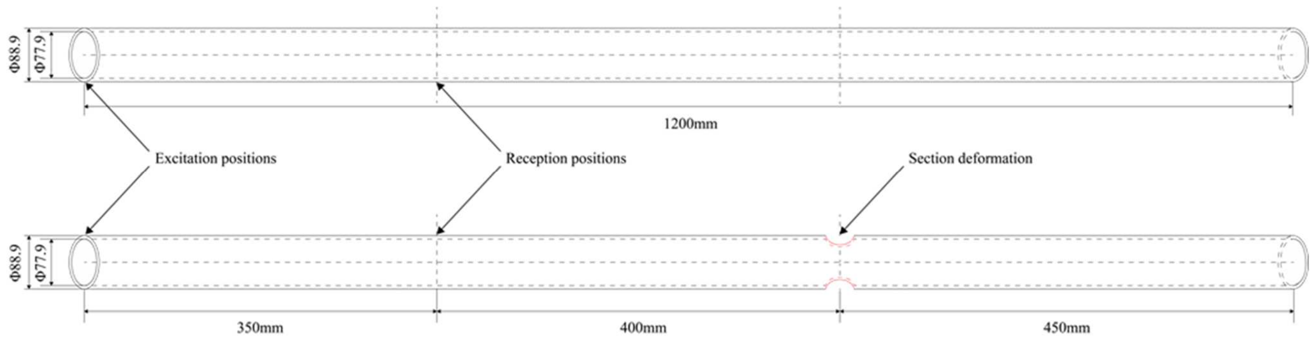

Fig. 3. Geometry of pipes without and with local deformations.

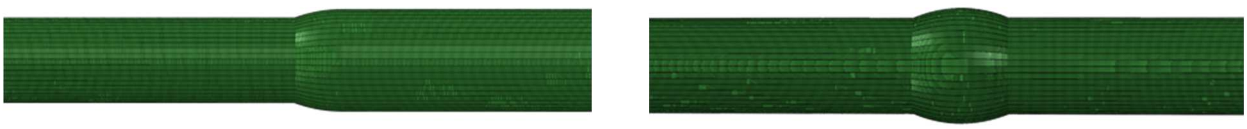

(a) (b)

Fig. 4. FE models of pipe with cross-sectional deformation: (a) arc slope model; (b) axisymmetric deformation model.

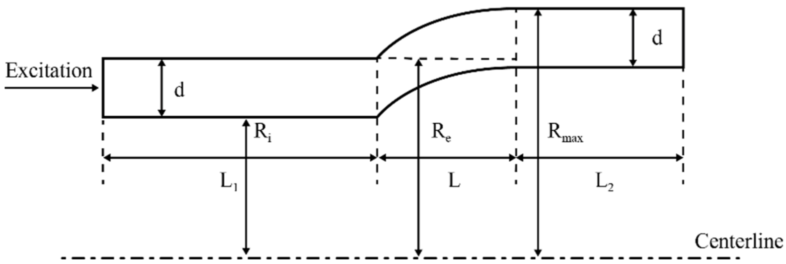

(a)

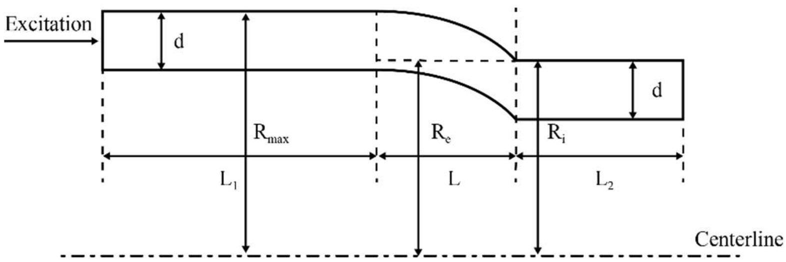

(b)

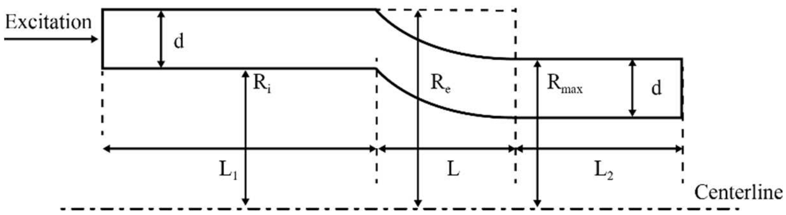

(c)

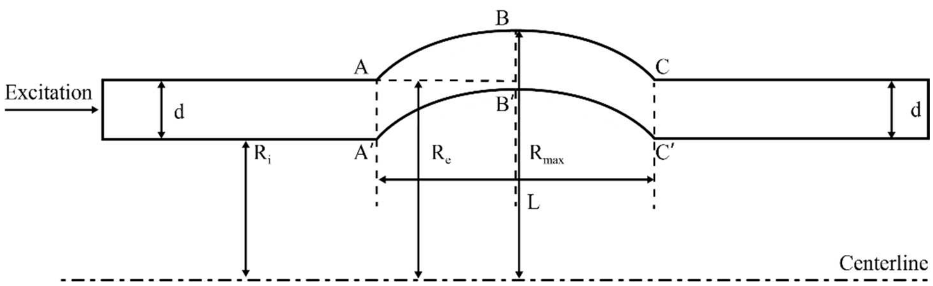

(d)

Fig. 5. Schematic of (a) bulge: arc slope-up; (b) bulge: arc slope-down; (c) dent: arc slope-down; (d) arced bulge.

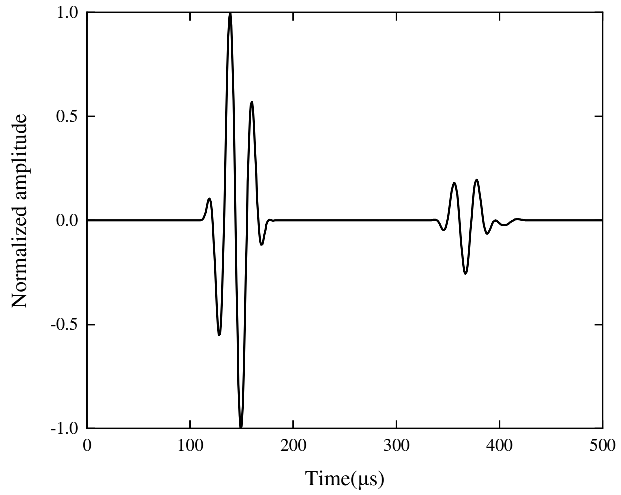

(a)

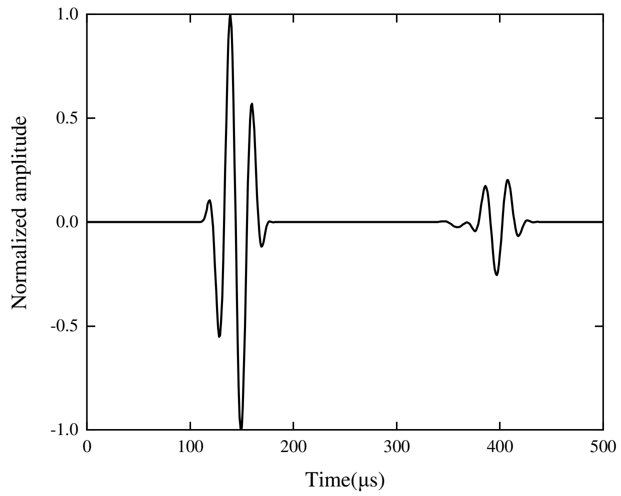

(b)

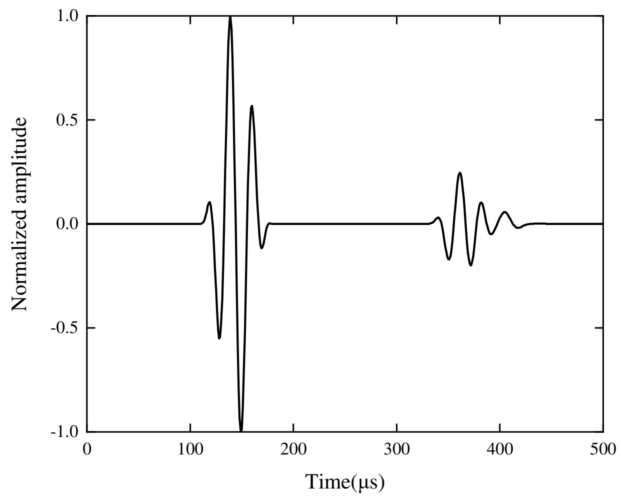

(c)

Fig. 6. Time domain signal for (a) bulge: slope-up; (b) bulge: slope-down; (c) dent: arc slope-down.

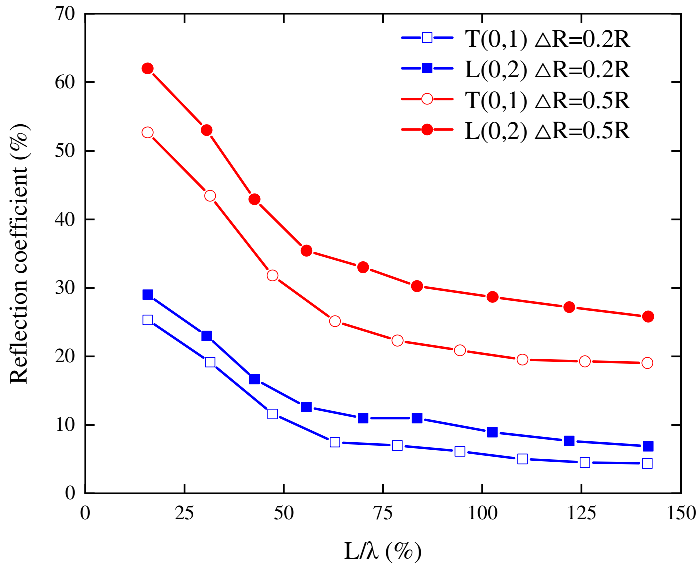

Fig. 7. Variation of the L(0,2) and T(0,1) mode reflection coefficients with the ratio of the axial extent of deformation to the wavelength.

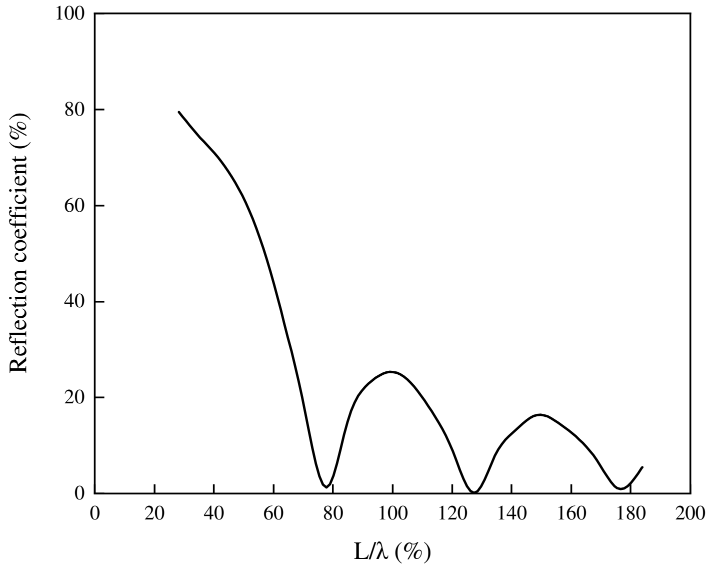

Fig. 8. Reflection coefficient for axisymmetric bulge deformation of varying axial extent. Results are for T(0,1) incident on a 3 inch pipe at 45kHz and ΔR=10mm (22.5% radius).

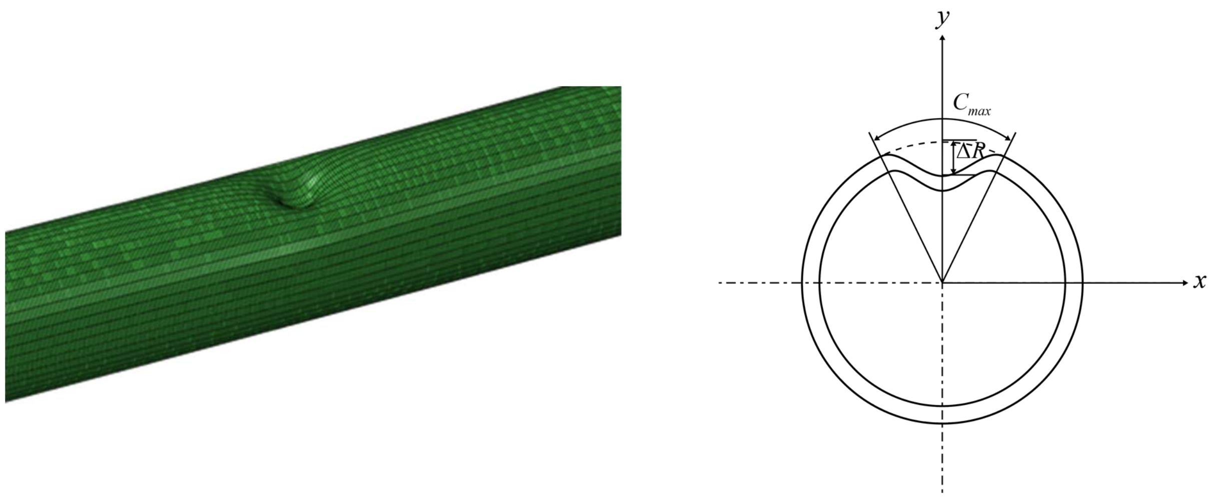

(a) (b)

Fig. 9. Modelling of pipe with cross-sectional dent deformation: (a) FE non-axisymmetric deformation model; (b) Schematic of a non-axisymmetric dent.

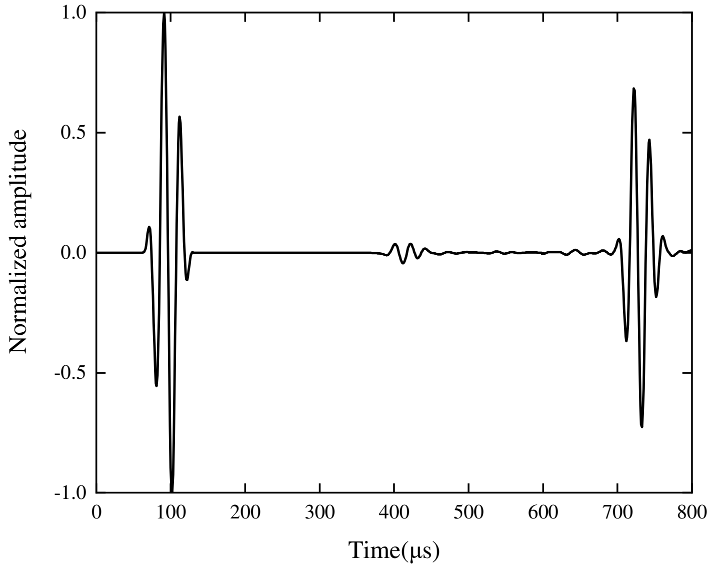

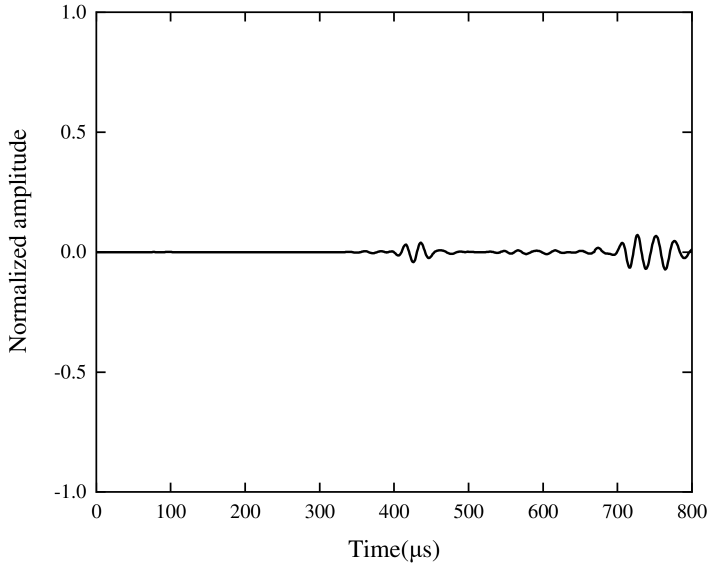

Fig. 10. Typical processed reflected signals from the FEM model (C_{max}=45° , ΔR=14.5mm); (a) Order 0 (axisymmetric) signals; (b) Order 1 signals.

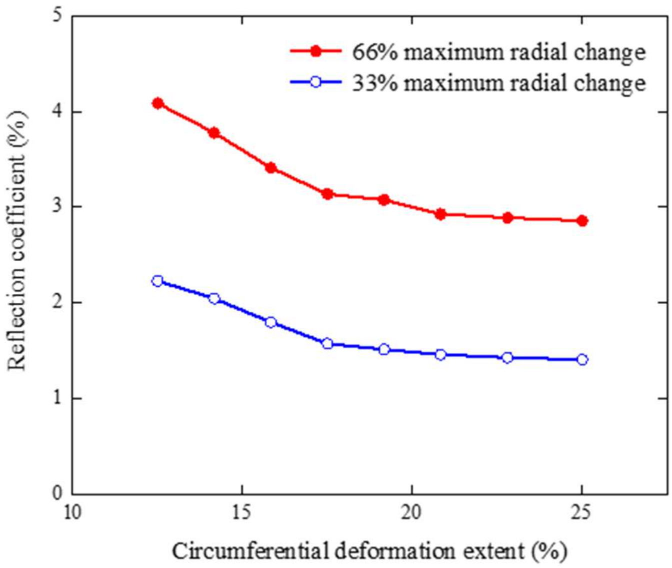

Fig. 11. Variation of the F(1,3) mode reflection coefficient with the percentage of the circumferential extent of deformation: (a) 33% and (b) 66% maximum radial change.

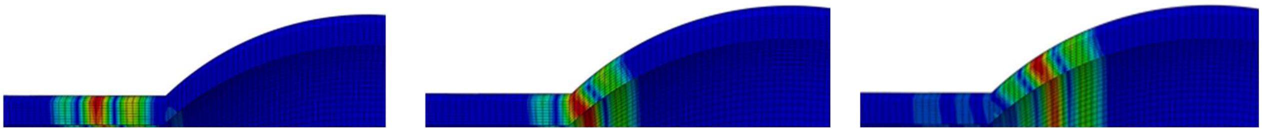

(a) (b) (c)

Fig. 12. Snapshots of the contour for total displacement magnitude at different time from FE results: (a) incident L(0,2) mode before interacting with deformation; (b) incident L(0,2) mode at the deformation; (c) reflected L(0,2) mode from the deformation.

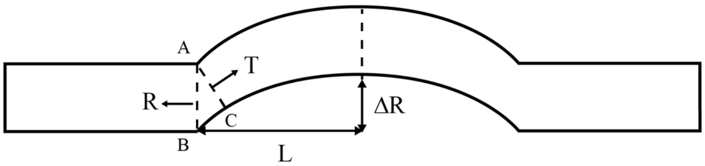

Fig. 13. Schematic of deformation case to explain reflection and transmission characteristics at the deformation section.

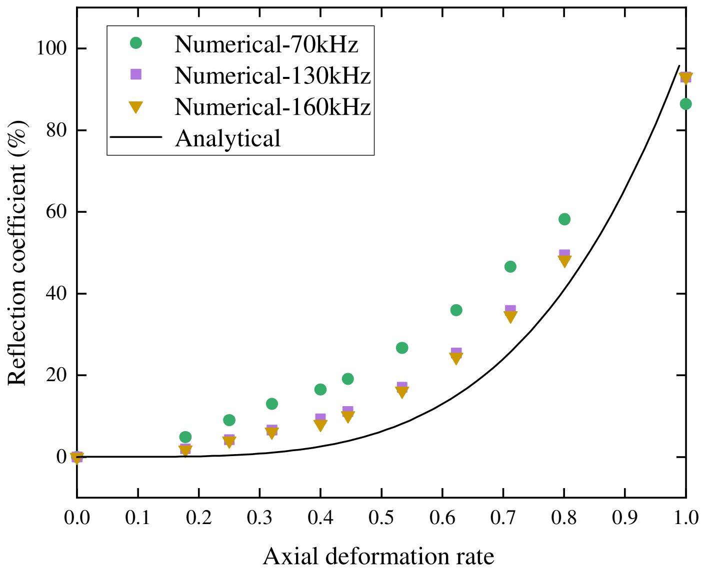

Fig. 14. Variation of the L(0,2) mode reflection coefficient with the rate of the axial extent of deformation.

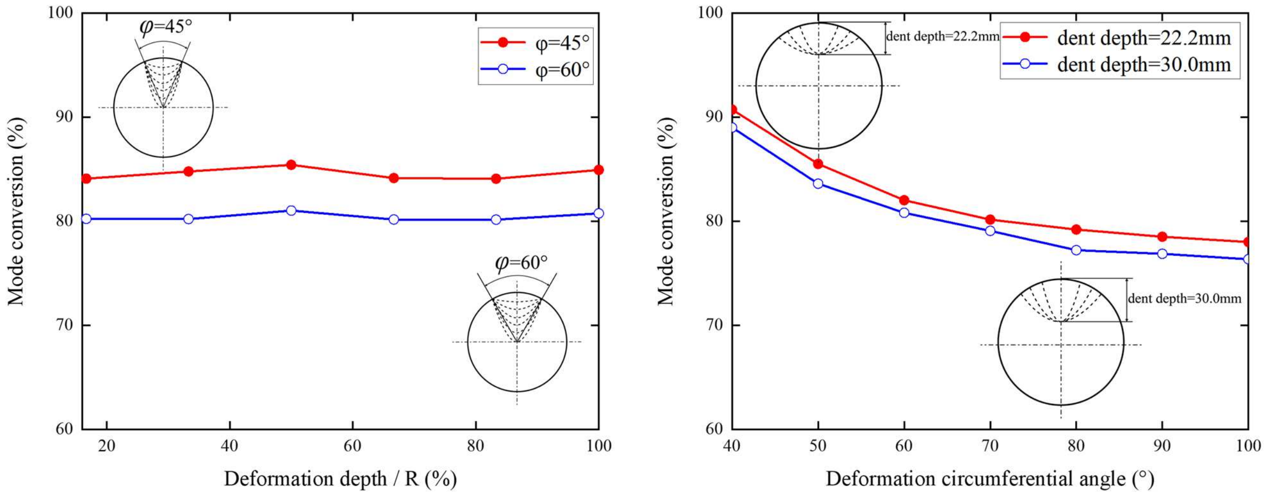

(a) (b)

Fig. 15. Variation of the mode conversion ratio with the (a) deformation depth; (b) circumferential extent of deformation.

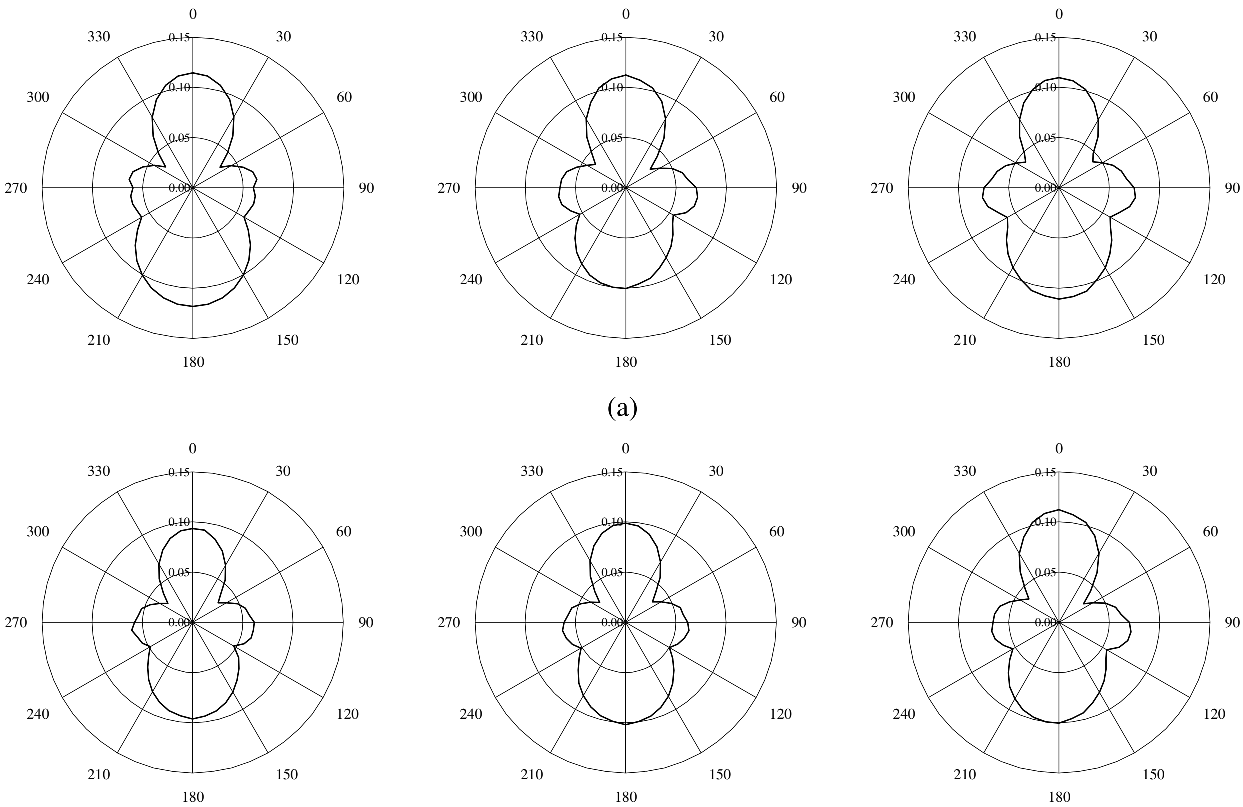

(a)

(b)

Fig. 16. Angular profiles of L(0,2) resulting from the detection signals at 230kHz for dent (a) with different circumferential extent 45°, 60°, 75°; (b) with different deformation depth 0.15R, 0.35R, 0.5R.

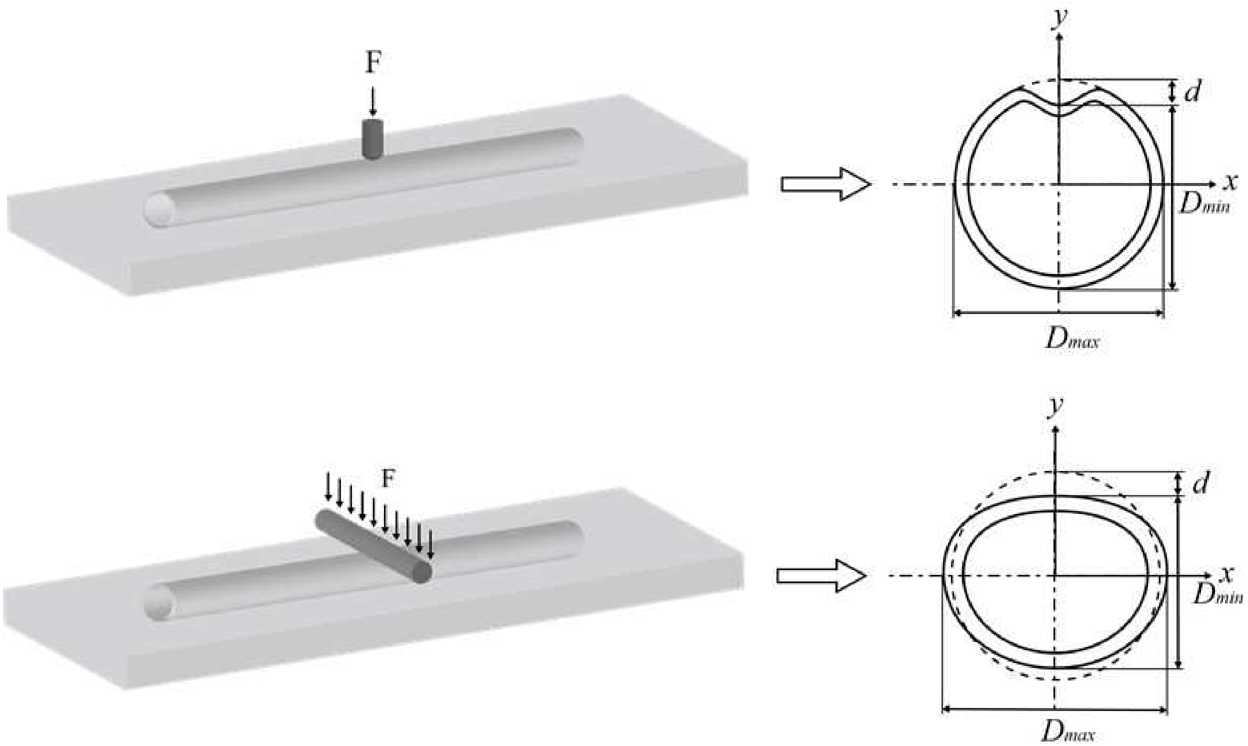

Fig. 17. Schematic of two types of deformation manufacturing processes.

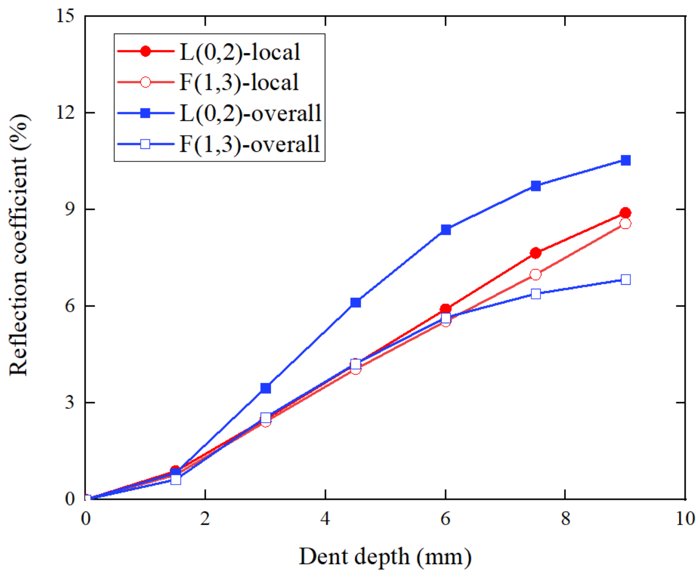

Fig. 18. Reflection coefficients for both types of deformation in 20mm diameter, 1mm wall thickness steel pipe at 230kHz as a function of dent depth.

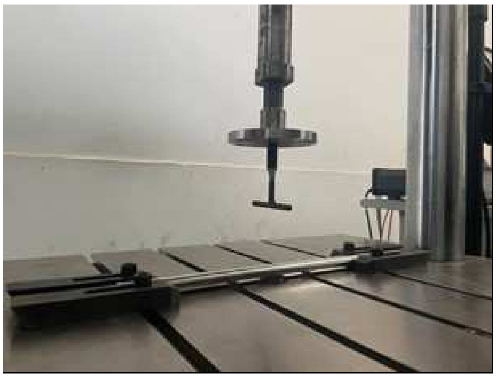

(a)

(b)

Fig. 19. Fabrication of pipe deformations (a) fabrication Setup; (b) typical local and overall deformation profiles (dent depth=8.5mm)

Fig. 20. Photo of the inspection system setup

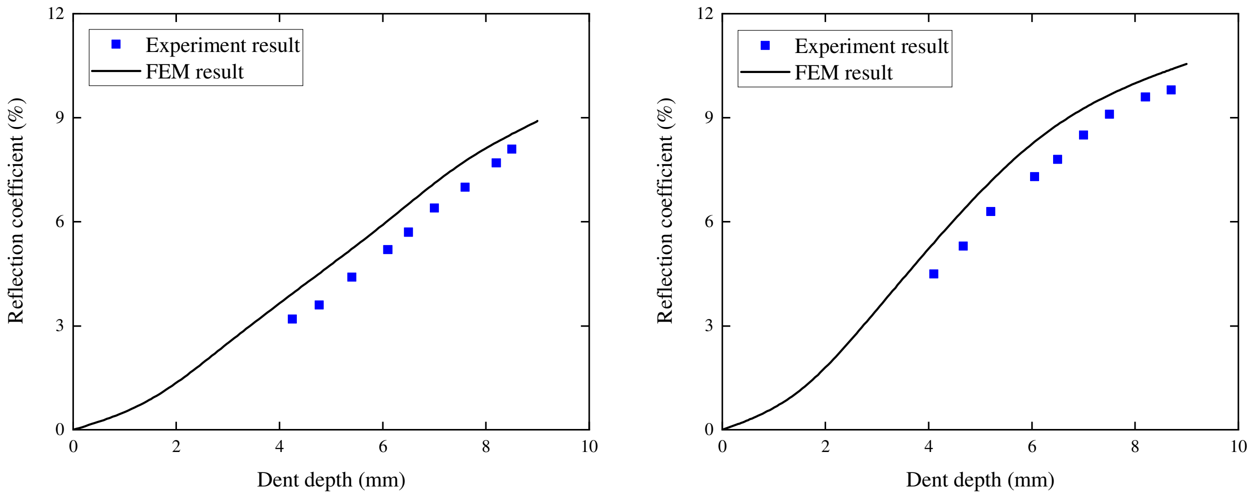

(a) (b)

Fig. 21. Comparison between FE (lines) and experiments (square dots) with cross-sectional deformation for the L((0,2) mode (a) Variation in RC of deformation with local deformation depth; (b) Variation in RC of deformation with overall deformation depth

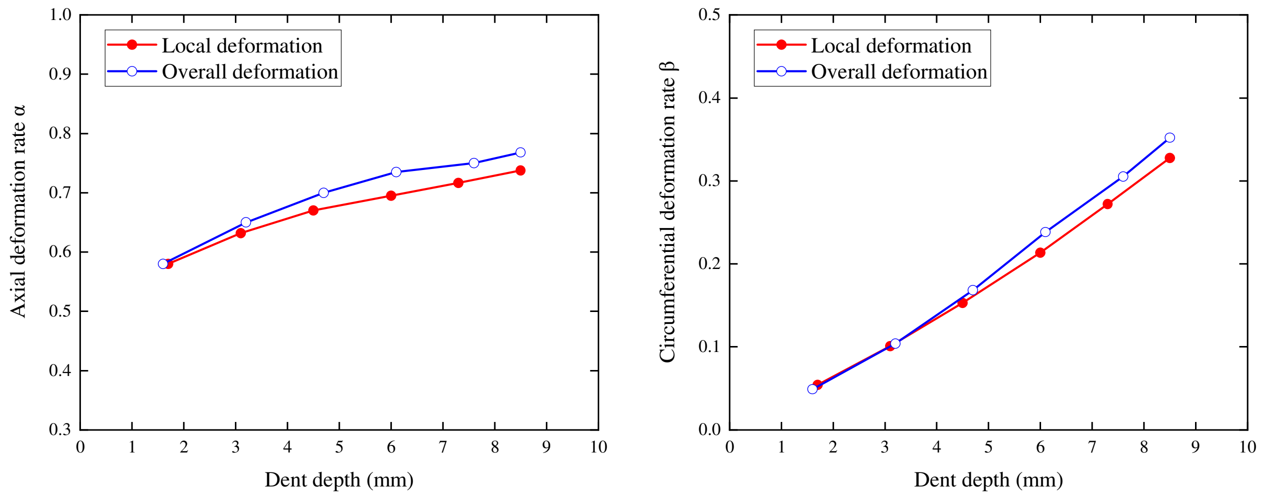

(a) (b)

Fig. 22. Variation of deformation parameters with dent depth (a) axial deformation rate δ ; (b) circumferential deformation rate β.

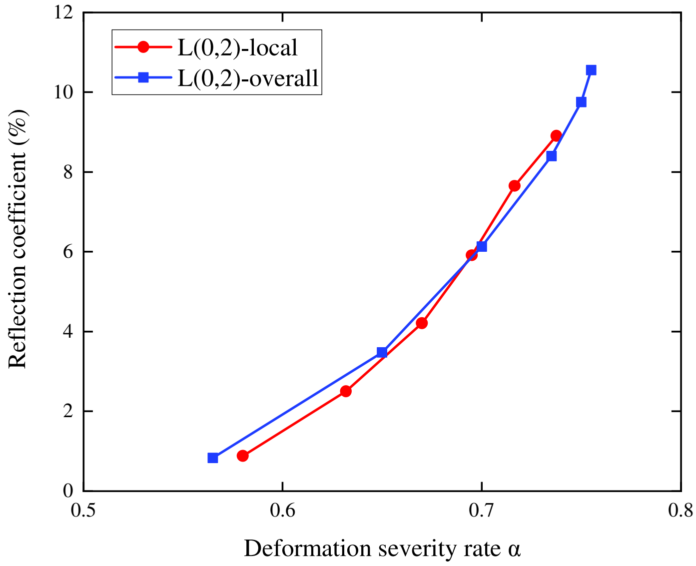

Fig. 23. Variation of the L(0,2) mode reflection coefficient with the deformation severity rate δ.

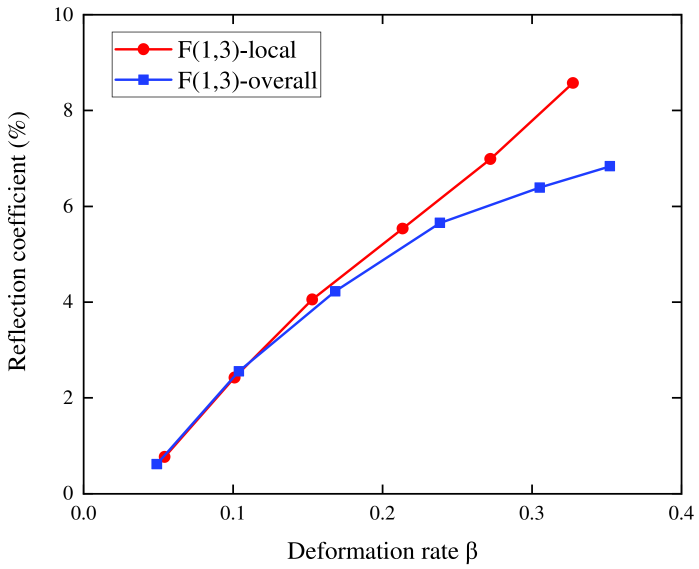

Fig. 24. Variation of the F(1,3) mode reflection coefficient with the deformation rate β.

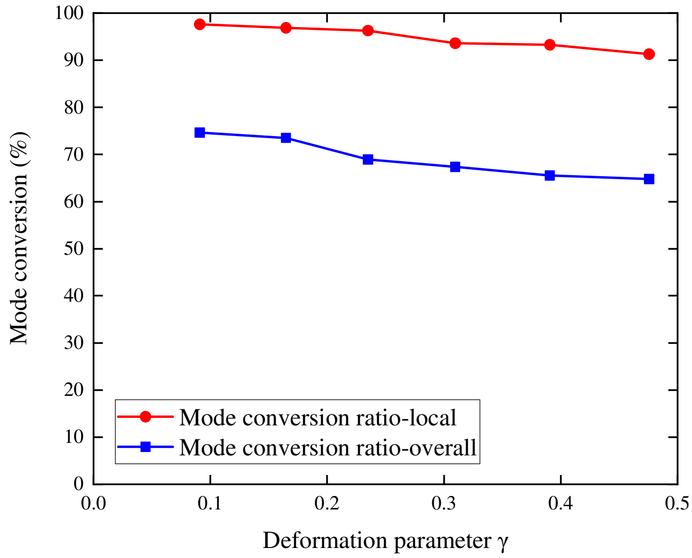

Fig. 25. Variation of the mode conversion ratio with the deformation rate γ.